Electronic Supplementary Material (ESI) for Journal of Materials Chemistry A.
This journal is © The Royal Society of Chemistry 2016

Supporting Information

for

Iron oxide/porous carbon as a heterogeneous Fenton catalyst for fast decomposition of hydrogen peroxide and efficient removal of methylene blue

Seung Hwa Yoo[a], Dawon Jang[a,b], Han-Ik Joh[a,b], and Sungho Lee[a,b]*

Carbon Convergence Materials Research Center, Institute of Advanced Composite Materials, Korea Institute of Science and Technology, Chudong-ro, Bongdong-eup, Wanju-gun, Jeollabuk-do 565-905, Republic of Korea

Department of Nanomaterials Engineering, Korea University of Science and Technology,217 Gajeong-ro, Tuseong-gu, Daejeon, 305-350 Republic of Korea

E-mail: sunghol@kist.re.kr

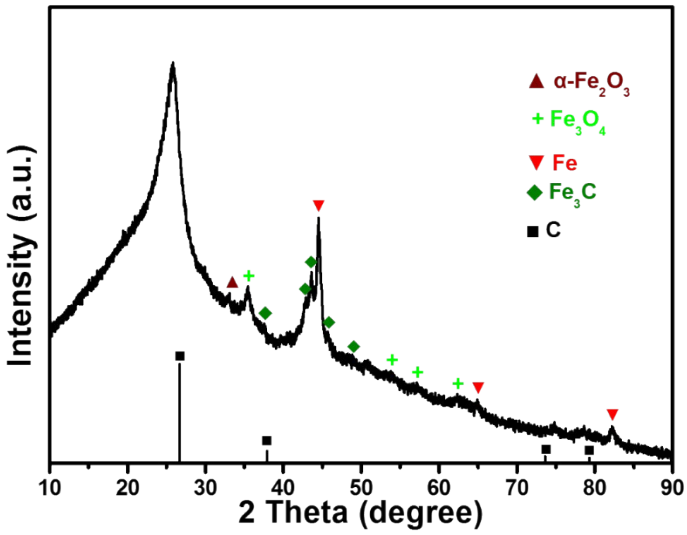

Figure S1. X-ray diffraction (XRD) pattern of Fe_3O_4/Fe/Fe_3C@PCNF.

The XRD pattern of Fe_3O_4/Fe/Fe_3C@PCNF is shown in Figure S1, revealing that various diffraction peaks were observed. The most intense diffraction peak was located at 2θ = 25.84°, which originated from the graphitic structure of PCNF. Interestingly, the 2θ of PCNF was lower than the 2θ of graphite (002) plane (2θ = 26.38°, JCPDS No. 41-1487). The d-spacing was calculated as 3.44 Å, which well matches with the TEM observation. From this observation, the graphitic structure of PCNF was implied to not be perfect graphite; rather, it has a graphitic structure with larger d-spacing. In addition to the graphitic diffraction peak, various diffraction peaks were derived from the catalyst particle Fe_3O_4/Fe/Fe_3C. The most intense diffractions could be observed by α-Fe (2θ = 44.67, 65.02, and 82.33°, JCPDS No. 06-0696) and Fe_3C (2θ = 37.65, 42.87, 43.74, 45.85, and 49.10°, JCPDS No. 34-0001). Fe_3O_4 (2θ = 35.42, 53.39, 56.94, and 62.52°, JCPDS No. 19-0629) was also detected with a trace amount of α-Fe_2O_3 (2θ = 33.15°, JCPDS No. 33-0664).

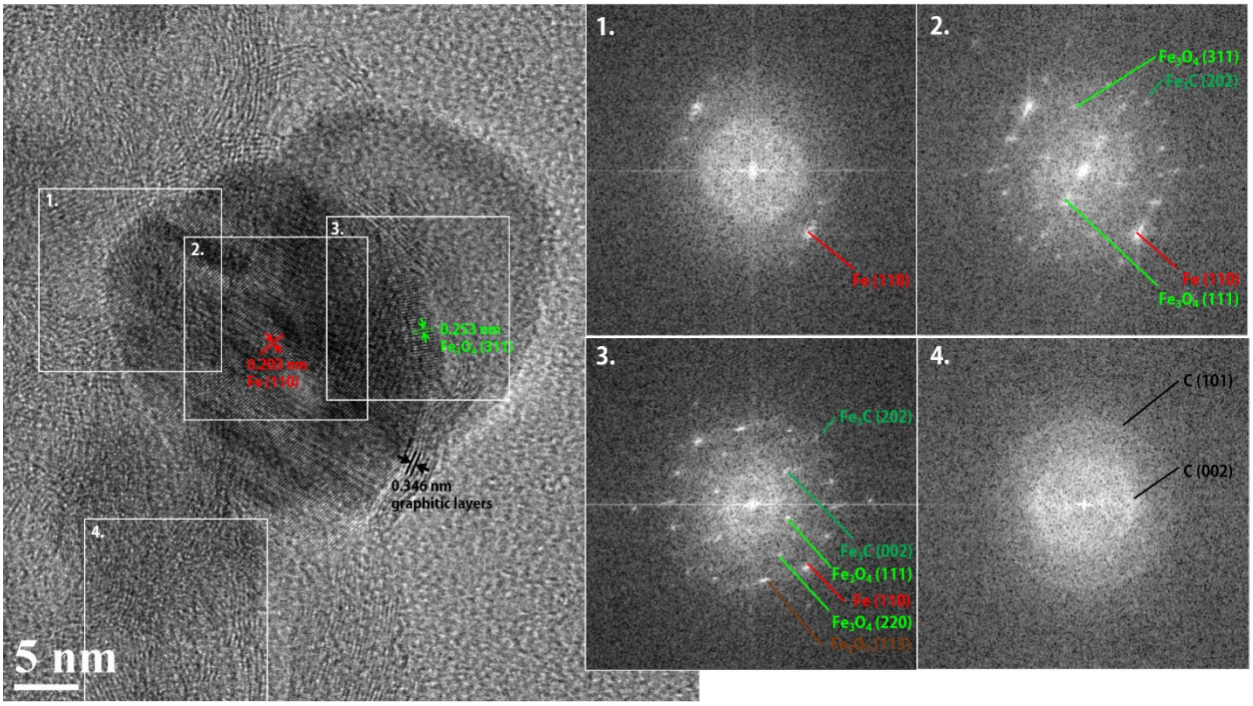

Figure S2. High resolution-TEM image of catalyst nanoparticles located at the outermost edge of Fe_3O_4/Fe/Fe_3C@PCNF and its corresponding fast Fourier transform (FFT) patterns at the different regions selected.

The FFT patterns of Fe_3O_4/Fe/Fe_3C@PCNF were analyzed by changing the selected regions of the high-resolution TEM image. Regions 1, 2, and 3 were selected to observe the phases at different positions of Fe_3O_4/Fe/Fe_3C. In region 1, only Fe (110) was observable, i.e., the phase of catalyst particle most deeply embedded in PCNF was α-Fe. However, in region 2, diffractions of Fe_3O_4 (311), (111) and Fe_3C (202) were detected along with Fe (110). Hence, by moving toward the surface of Fe_3O_4/Fe/Fe_3C@PCNF (region 1 → 2), iron oxide starts to be observed in the catalyst particle. Finally, in region 3, additional diffraction peaks of Fe_3O_4 (220), Fe_3C (002), and α-Fe_2O_3 (113) were observed. Therefore, it is evident that Fe_3O_4 exists near the surface side of Fe_3O_4/Fe/Fe_3C@PCNF and that Fe exists closer to the central region of

Fe_3O_4/Fe/Fe_3C@PCNF. In region 4, the diffusive ring patterns of C (002) and (101) reflect the existence of a graphitic structure developed in PCNF.

Table S1. Rate constants of various iron oxide (1-11), iron oxide composite (12-13), and supported iron oxide (14-19) catalysts studied by other groups.

	Catalyst	k_{obsd} [$\times 10^{-3}$ min^{-1}]	k_{mass} [$\times 10^{-3}$ min^{-1} $(g/L)^{-1}$]	k_{mass} [M^{-1} s^{-1}]	pH	Reference
1	Goethite (α-FeOOH)	9.8 ± 1.0	19.6 ± 2.0	0.019-0.067	5-10	Environ. Sci. Technol. **1998**, 32, 1417-1423
2	Goethite	0.530	0.530	-	6.4	Water Res. **2001**, 35, 2291-2299
3	Goethite	13	0.001	-	7.7	J. Environ. Eng. **1998**, 124, 31-38
4	Hematite (α-Fe_2O_3)	26.4	26.4	-	6.3-6.5	J. Am. Chem. Soc. **2007**, 129, 10929-10936
5	Hematite	0.083	-	-	5.94	Water Res. **2001**, 35, 2291-2299
6	Hematite	143	143	-	6.3-6.5	J. Mater. Chem. A, **2016**, 4, 596-604
7	Ferrihydrite	15	0.012		7.7	J. Environ. Eng. **1998**, 124, 31-38
8	Ferrihydrite (granular)	9.0	-	-	8.00	Water Res. **2001**, 35, 2291-2299
9	Ferrihydrite	7.6	0.0151	-	7.0	J. Environ. Eng. **1998**, 124, 31-38
10	Magnetite (Fe_3O_4)	0.23	-	-	5.5	J. Nanopart. Res. **2012**, 14, 956-965
11	Magnetite	0.001 M	-	-	5.5	Chemosphere, **2005**, 60, 1118-1123
12	Fe^0/Fe_3O_4	≈ 30	≈ 7	-	5.3-5.7	Appl. Catal. B **2008**, 83, 131-139
13	Fe–Pt	23	-	-	5.5	J. Nanopart. Res. **2012**, 14, 956-965
14	α-Fe_2O_3 (plate) + Fe (II)	95.5	-	-	4.7	Appl. Catal. B **2016**, 181, 127-137
15	α-Fe_2O_3 (rod) + Fe (II)	143.6	-	-	4.7	Appl. Catal. B **2016**, 181, 127-137
16	Immobilized iron oxide	1.8	-	-	4	Appl. Catal. A **2008**, 346, 140-148
17	Fe_2O_3/Al_2O_3	-	-	0.037	12	J. Phys. Chem. **1978**, 82, 1505-1509
18	Fe_2O_3/Al_2O_3	-	-	0.013-0.031	9	Int. J. Chem. Kinet. **1990**, 22, 963-974.
19	Fe_2O_3/Al_2O_3/mesoporous SiO_2	0.782	3.91	-	4.1	Chem. Commun. **2006**, 463-465
20	Fe_3O_4/MWCNT	1.44	0.72	-	5.0	Appl. Catal. B **2011**, 107, 274-283
21	Fe_3O_4/mesoporous carbon	< 0.44	< 4.4	-	3.0	Chemosphere **2012**, 89, 1230-1237
22	Support–iron oxide	0.22	0.022	-	5.4	Appl. Catal. A **1999**, 185, 237-245
23	**Fe_3O_4/Fe/Fe_3C@PCNF**	**604.28**	**839.8**	**7.776**	**5.8-5.9**	**This work**

1. $[H_2O_2]_0$ = 0.0011-0.011 M, [catalyst] = 0.2-3 g/L,

2. $[H_2O_2]_0$ = 0.98-17.8 mM, [catalyst] = 1 g/L,

3. $[H_2O_2]_0$ = 500 mg/L, [catalyst] = 12500 mg/L,

3. $[H_2O_2]_0$ = 500 mg/L, [catalyst] = 0.5-12.5 g/L,

4. $[H_2O_2]_0$ = 0.02 M, [catalyst] = 1 g/L,

5. $[H_2O_2]_0$ = 0.98-17.8 mM, [catalyst] = 1 g/L,

6. $[H_2O_2]_0$ = 0.02 M, [catalyst] = 1 g/L,

7. $[H_2O_2]_0$ = 500 mg/L, [catalyst] = 1250 mg/L,

8. $[H_2O_2]_0$ = 5.88 mM, [catalyst] = 1 g/L,

9. $[H_2O_2]_0$ = 500 mg/L, [catalyst] = 500 mg/L,

10. $[H_2O_2]_0$ = 3.5%, [catalyst] = 5 ppm,

11&12. $[H_2O_2]_0$ = 2.7 M, catalyst = 30 mg,

13. $[H_2O_2]_0$ = 3.5%, [catalyst] = 5 ppm,

14&15. $[H_2O_2]_0$ = 0.05 mM, [catalyst] = 0.4 g/L,

16. $[H_2O_2]_0$ = 550 mg/L, catalyst = 20 g,

17. $[H_2O_2]_0$ = 7-15 cm^3/min, catalyst = 0.5-1.5 g,

18. $[H_2O_2]_0$ = 0.1 M, catalyst = 0.05 g,

19. $[H_2O_2]_0$ = 5 mM, [catalyst] = 0.2 g/L,

20. $[H_2O_2]_0$ = 5.3 mM, [catalyst] = 2 g/L,

21. $[H_2O_2]_0$ = 10 mM, [catalyst] = 0.1 g/L,

22. $[H_2O_2]_0$ = 23.5 mM, [catalyst] = 10 g/L,

23. $[H_2O_2]_0$ = 40 mM, [catalyst] = 0.125-0.75 g/L.

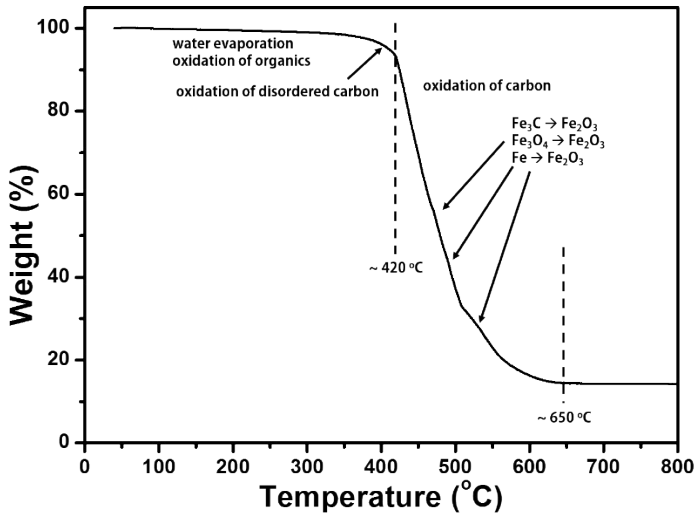

Figure S3. Thermogravimetric analysis (TGA) curve of Fe_3O_4/Fe/Fe_3C@PCNF measured in air.

The Fe content was calculated based on the TGA curve of Fe_3O_4/Fe/Fe_3C@PCNF. By heating Fe_3O_4/Fe/Fe_3C@PCNF in air, the adsorbed water molecules and organic matters were evaporated to cause slight but steady weight loss until ~ 300 °C. The ramp of weight loss, which increases at approximately 400-420 °C, is due to oxidation of the amorphous carbon part of Fe_3O_4/Fe/Fe_3C@PCNF [1]. Above 420 °C, the steepest weight loss response was observed; this response was attributed to the oxidation of graphitic carbon of Fe_3O_4/Fe/Fe_3C@PCNF until no weight change was observed at ~ 650 °C [2-4]. During the oxidation of carbon, iron species (Fe_3O_4, Fe, Fe_3C, and α-Fe_2O_3) of Fe_3O_4/Fe/Fe_3C@PCNF experienced oxidation, which led to the phase transition to iron oxides. The slight weight increase due to oxygen incorporation in these iron species could be observed as several bumps in the TGA curve (at ~ 460, 480, and 530 °C) [2-4]. In the temperature region of ~ 650 to 800 °C, no further weight loss occurred, with the remaining 14.31% being the residual material. This result can be explained as follows: when heating Fe_3O_4/Fe/Fe_3C@PCNF to 800 °C in air, all carbonaceous materials are oxidized and

evaporated, while iron species are oxidized to a stable iron oxide form, which remained as a residual material. It is well known that iron species ultimately oxidize to α-Fe_2O_3 under 800 °C heating in air; therefore, the residual material was assumed to be all α-Fe_2O_3 [5-8]. Considering the molecular weights of Fe and O and the stoichiometry of Fe_2O_3, it is conclusive that the Fe content of Fe_3O_4/Fe/Fe_3C@PCNF was 10.02%. Based on this observation, the k_{mass} was calculated to be 7.776 M^{-1} s^{-1}.

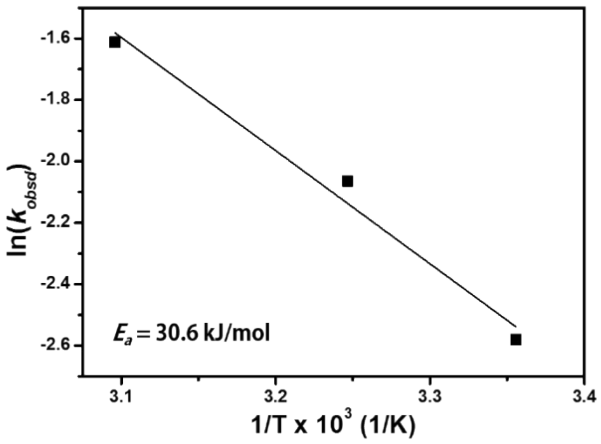

Figure S4. Arrhenius plot derived from H_2O_2 decomposition by Fe_3O_4/Fe/Fe_3C@PCNF performed at different solution temperatures (25, 35, and50 ℃).

The Arrhenius equation written below was utilized to evaluate the activation energy (E_a) of the catalytic reaction.

$$k = Ae^{-Ea/(RT)} \rightarrow \ln(k) = \frac{-Ea}{R}\left(\frac{1}{T}\right) + \ln(A) \quad (1)$$

The quantity ln(k_{obsd}) was plotted as function of 1/T, and a linear regression was taken by three values of k_{obsd} measured at 25, 35, and 50 ℃ (R^2 = 0.97). E_a was calculated as 30.6 kJ/mol from the slope (-E_a/R) of the linear regression line.

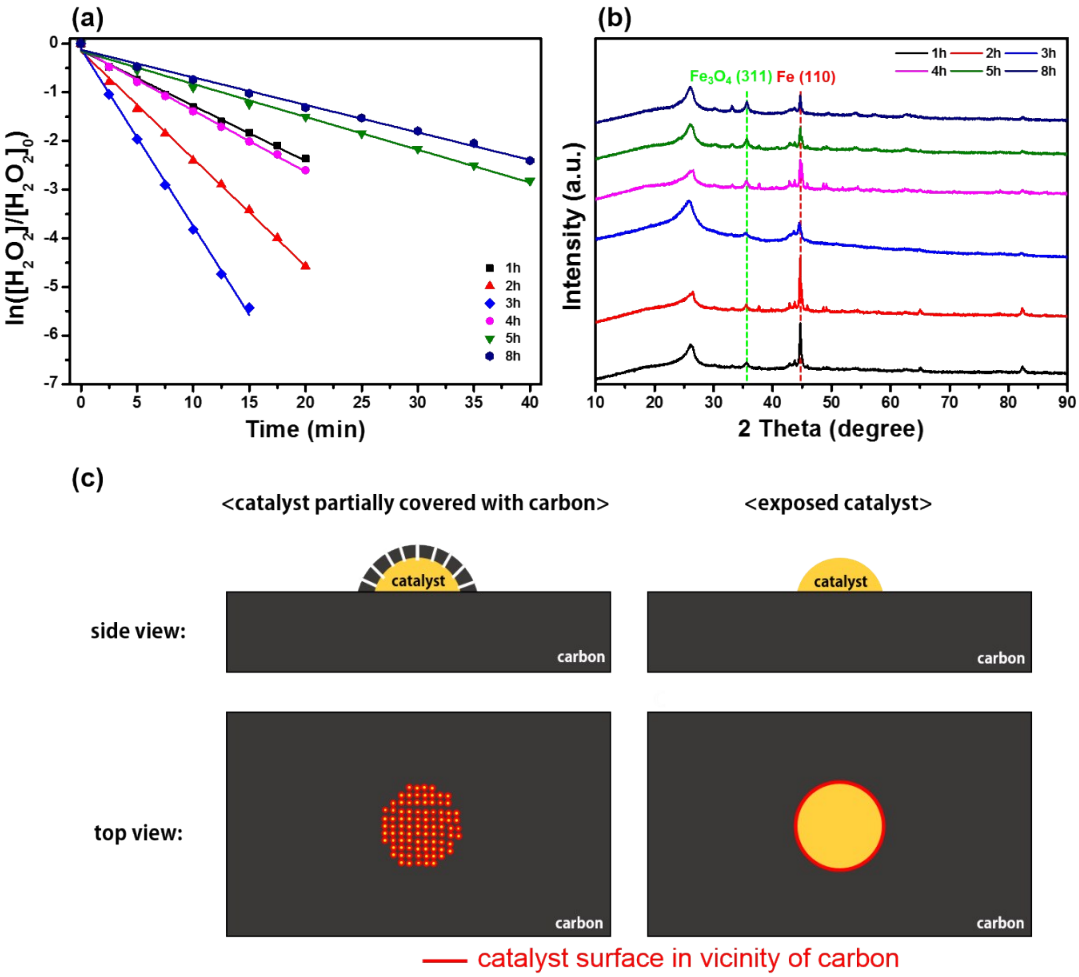

Figure S5. (a) $\ln([H_2O_2]/[H_2O_2]_0)$ vs. time plot and (b) XRD patterns of Fe_3O_4/Fe/Fe_3C@PCNF activated at 300 °C for different time durations. (c) Illustration for comprehensive understanding of the proposed mechanism.

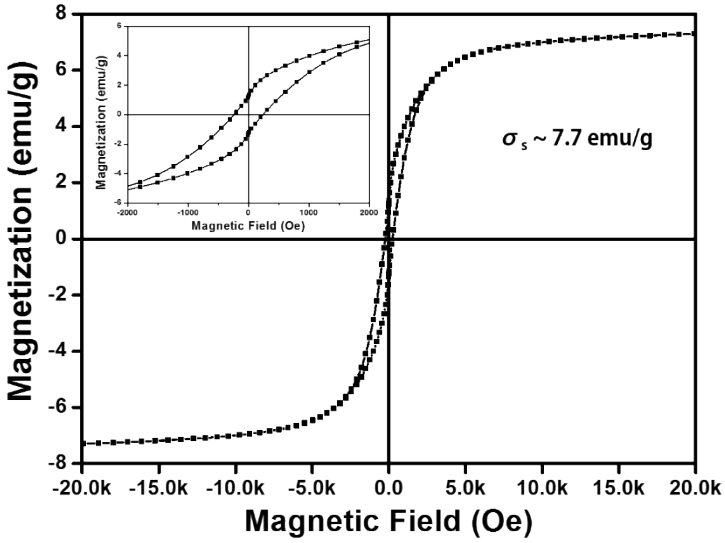

Figure S6. B-H curve of Fe_3O_4/Fe/Fe_3C@PCNF. Inset shows high magnification of -2 kOe to 2 kOe range.

The B-H curve exhibited a hysteresis loop that indicated the ferromagnetic behavior of Fe_3O_4/Fe/Fe_3C@PCNF. The saturation magnetization (σ_s) was estimated as 7.7 emu/g, which indicated that Fe_3O_4/Fe/Fe_3C@PCNF possessed a high enough magnetic moment to be separated by a magnet. The motion picture shows the efficient separation of Fe_3O_4/Fe/Fe_3C@PCNF by a magnet, which was dispersed in water after the H_2O_2 decomposition experiment.

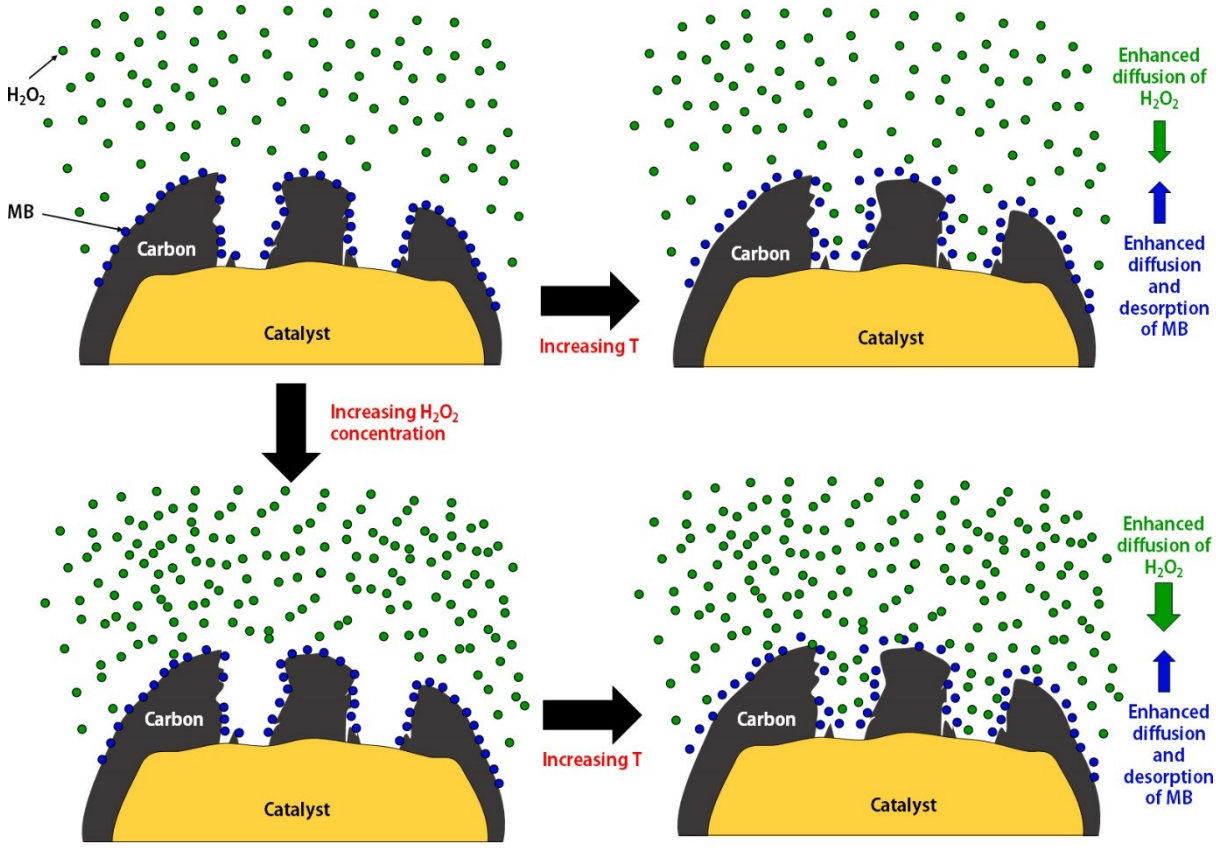

Figure S7. Representative illustration of MB catalytic removal with Fe_3O_4/Fe/Fe_3C@PCNF by increasing the solution temperature and H_2O_2 concentration.

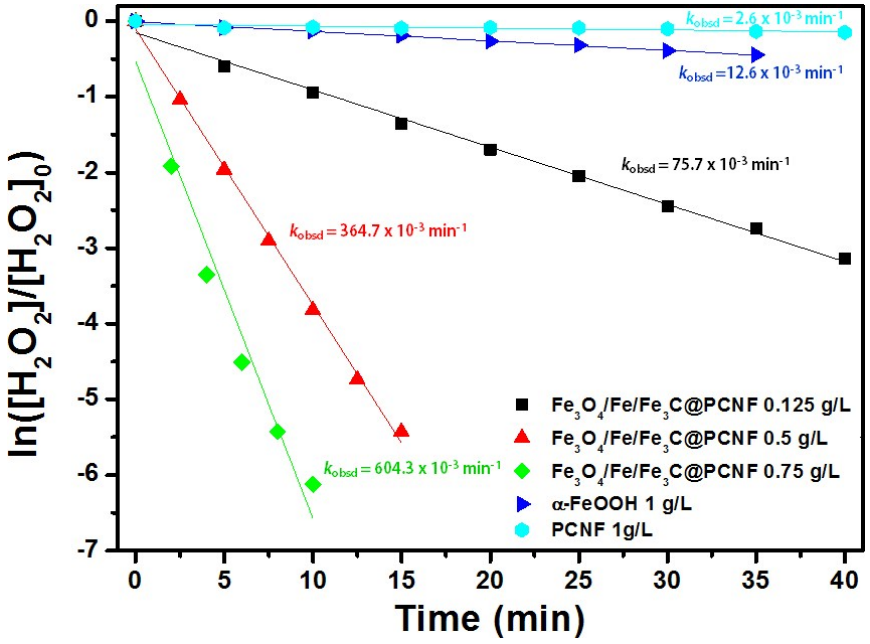

Figure S8. ln([H_2O_2]/[H_2O_2]$_0$) vs. time plot of α-FeOOH and PCNF (Fe_3O_4/Fe/Fe_3C@PCNF plotted for comparison).

The k_{obsd} of PCNF and α-FeOOH (goethite, catalyst grade, 30-50 mesh, Sigma-Aldrich) was measured to compare with Fe_3O_4/Fe/Fe_3C@PCNF. PCNF and α-FeOOH showed k_{obsd} = 2.6 × 10^{-3} and 12.6 × 10^{-3} min^{-1}, which were a relatively low value compared to Fe_3O_4/Fe/Fe_3C@PCNF. PCNF was fabricated by the same procedure explained in the experimental section without including the iron acetylacetonate.

The radical species produced from H_2O_2 decomposition with Fe_3O_4/Fe/Fe_3C@PCNF at room temperature was observed by EPR method. For the experiment, 1 g/L of Fe_3O_4/Fe/Fe_3C@PCNF was added in 0.32 M H_2O_2 aqueous solution and an extraction was taken immediately and 10 min after the reaction was started. After filtering Fe_3O_4/Fe/Fe_3C@PCNF from the extraction, 5, 5-dimethyl-1-pyrroline N-oxide (DMPO) was added as a spin trapping agent. Figure R1 shows the EPR signal of the radical species detected by EPR. The EPR spectra displayed a 4-fold peak with intensity ratio of 1:2:2:1. Furthermore, the hyperfine splitting constant a_N and a_H^{β} was equivalent as 15 G. From these facts, it was verified that DMPO-OH• adduct was detected, indicating that hydroxyl radicals (OH•) were mainly formed by decomposition of H_2O_2 with Fe_3O_4/Fe/Fe_3C@PCNF at room temperature [Chem. Eng. J., 2014, 236, 251].

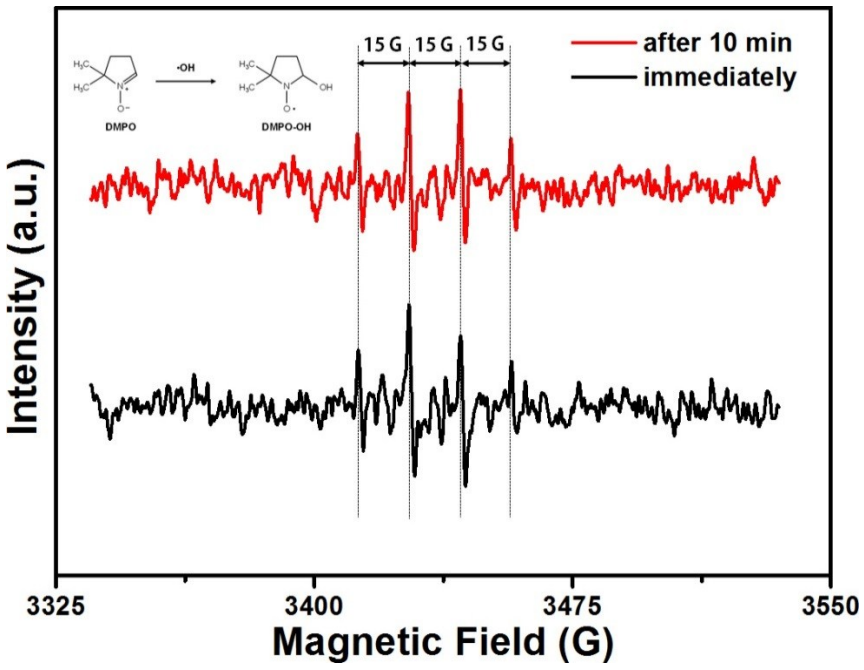

Figure S9. EPR spectra of DMPO-OH• adduct derived from OH• which was formed by H_2O_2 decomposition with Fe_3O_4/Fe/Fe_3C@PCNF.

The blank test for MB adsorption was conducted by adding Fe_3O_4/Fe/Fe_3C@PCNF in the MB solution (100 mg/L, 85 ℃) without adding H_2O_2. As shown in Figure R2, around 75% of MB was removed by adsorption within 10 min and small amounts were gradually removed afterward. Therefore, it was verified that the adsorptive removal was nearly saturated within 30 min before adding H_2O_2 according to our experimental procedure. The blank test for MB removal by H_2O_2 thermal decomposition was conducted by adding 0.32 M H_2O_2 in the MB solution (100 mg/L) at 85 ℃ (Figure R2). The MB concentration did not change during the experiment, which indicated that the thermal decomposition of H_2O_2 did not lead to MB removal.

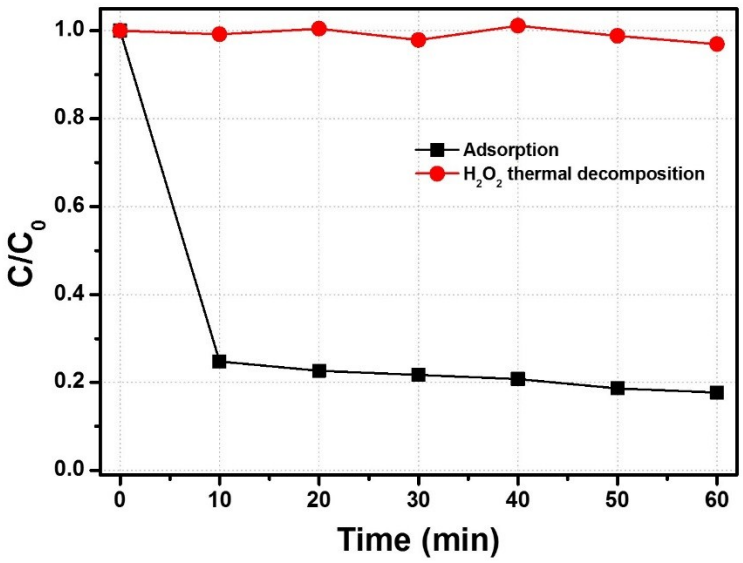

Figure S10. Removal curve of MB with Fe_3O_4/Fe/Fe_3C@PCNF prepared by activation at 300 ℃ for 8 h. The adsorption was conducted at 85 ℃. The H_2O_2 thermal decomposition test was conducted for 0.32 M H_2O_2 at 85 ℃.

The pH 5.4 and 4.5 was the natural pH when 0.04 and 0.32 M H_2O_2 was added to MB solutions, respectively. Additional experiments were conducted to compare the results at the same pH conditions. The pH 4.5 was chosen for these experiments which was the natural pH of MB solution with addition of 0.32 M H_2O_2. In case of 0.04 M H_2O_2, the pH was adjusted to 4.5 by adding appropriate amount of HCl. The MB removal curves are shown in Figure R4a and b for two samples (Fe_3O_4/Fe/Fe_3C@PCNF prepared by activation at 300 ℃ for 3 h and 8 h). At the same pH 4.5 condition, the removal of MB was higher in case of 0.32 M H_2O_2 compared to 0.04 M H_2O_2 for both samples. Based on this result, it was once more verified that the removal of MB was enhanced by increasing the H_2O_2 concentration from 0.04 to 0.32 M for Fe_3O_4/Fe/Fe_3C@PCNF at the same pH condition. The pH change during MB removal was tracked and is shown in Figure 3c. According to the mineralization of MB (1),

$$C_{16}H_{18}N_3SCl\ (MB) + 52H_2O_2 \rightarrow 16CO_2 + 0.5O_2 + 58H_2O + 3HNO_3 + H_2SO_4 + HCl \quad (1)$$

the consumption of H_2O_2 led to the formation of acidic products (HNO_3, H_2SO_4, and HCl). Therefore, the pH was gradually decreased to ~ 4.1 after 30 min.

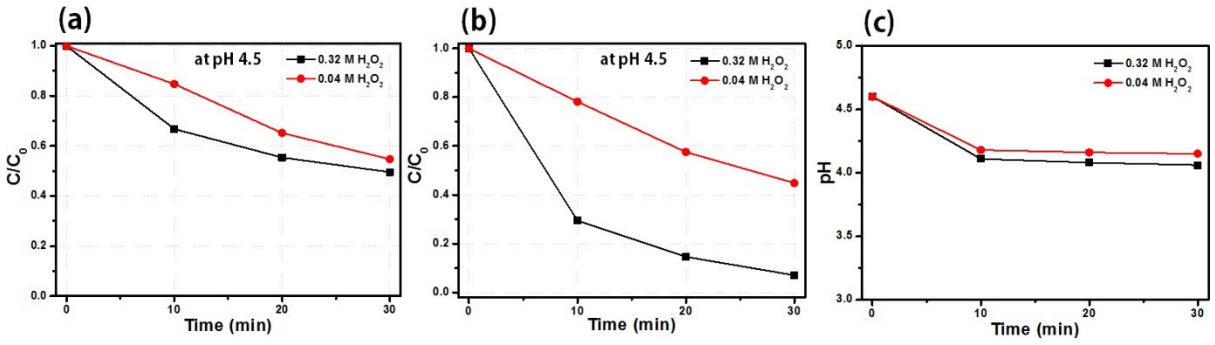

Figure S11. Removal curve of MB with Fe_3O_4/Fe/Fe_3C@PCNF prepared by activation at 300 ℃ for (a) 3 h and (b) 8 h tested at different H_2O_2 concentrations. The experiment was conducted at 25 ℃ and initial pH 4.5. (c) The pH plot of (b).

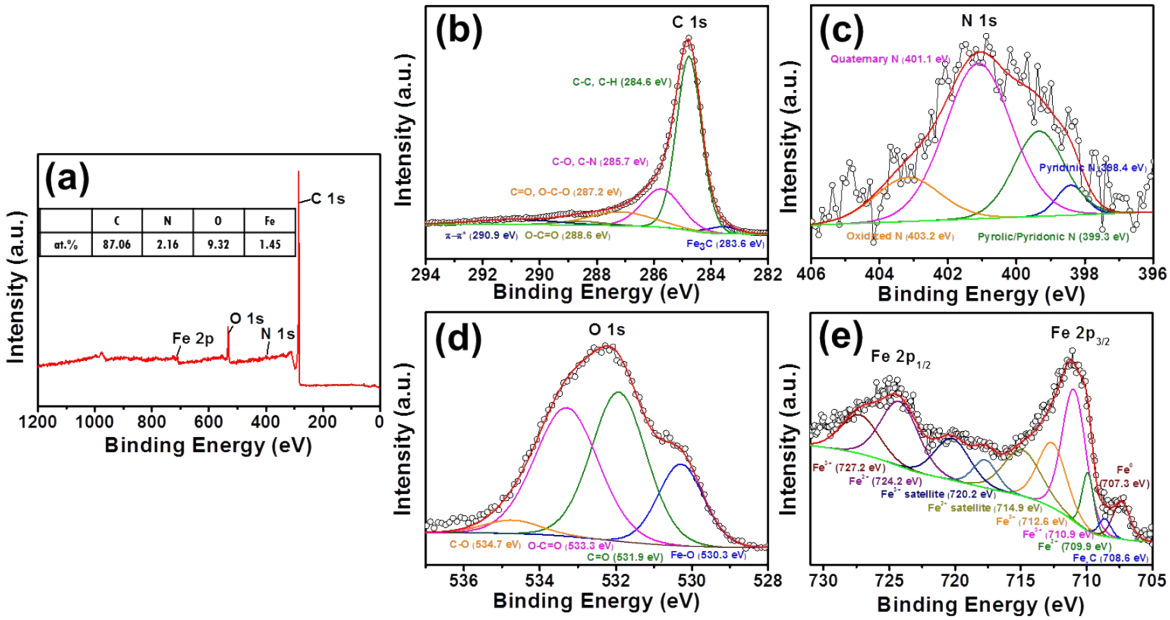

Figure S12. X-ray photoelectron spectra of Fe_3O_4/Fe/Fe_3C@PCNF activated at 300 tra of Fea(a) Survey scan, peak deconvolution of (b) C1s, (c) N1s, (d) O1s, and (e) $Fe2p_{1/2}$ & $Fe2p_{3/2}$. All deconvoluted peaks are assigned with its chemical bonds.

References

[1] K.L. Strong, D.P. Anderson, K. Lafdi, J.N. Kuhn, Purification process for single-wall carbon nanotubes, carbon, 41 (2003) 1477-1488.

[2] Y.-G. Huang, X.-L. Lin, X.-H. Zhang, Q.-C. Pan, Z.-X. Yan, H.-Q. Wang, J.-J. Chen, Q.-Y. Li, Fe 3 C@ carbon nanocapsules/expanded graphite as anode materials for lithium ion batteries, Electrochimica Acta, 178 (2015) 468-475.

[3] Y. Hu, J.O. Jensen, W. Zhang, L.N. Cleemann, W. Xing, N.J. Bjerrum, Q. Li, Hollow spheres of iron carbide nanoparticles encased in graphitic layers as oxygen reduction catalysts, Angewandte Chemie International Edition, 53 (2014) 3675-3679.

[4] F. Magalhães, M. Pereira, J. Fabris, S. Bottrel, M. Sansiviero, A. Amaya, N. Tancredi, R. Lago, Novel highly reactive and regenerable carbon/iron composites prepared from tar and hematite for the reduction of Cr (VI) contaminant, Journal of hazardous materials, 165 (2009) 1016-1022.

[5] S. Zhang, M. Zeng, J. Li, J. Li, J. Xu, X. Wang, Porous magnetic carbon sheets from biomass as an adsorbent for the fast removal of organic pollutants from aqueous solution, Journal of Materials Chemistry A, 2 (2014) 4391-4397.

[6] J. Wang, H. Zhou, J. Zhuang, Q. Liu, Magnetic γ-Fe 2 O 3, Fe 3 O 4, and Fe nanoparticles confined within ordered mesoporous carbons as efficient microwave absorbers, Physical Chemistry Chemical Physics, 17 (2015) 3802-3812.

[7] C. Fu, A. Mahadevegowda, P.S. Grant, Fe 3 O 4/carbon nanofibres with necklace architecture for enhanced electrochemical energy storage, Journal of Materials Chemistry A, 3 (2015) 14245-14253.

[8] M. Krajewski, K. Brzozka, W. Lin, H. Lin, M. Tokarczyk, J. Borysiuk, G. Kowalski, D. Wasik, High temperature oxidation of iron–iron oxide core–shell nanowires composed of iron nanoparticles, Physical Chemistry Chemical Physics, 18(2016) 3900-3909.

[9] X. Zhang, Y. Ding, H. Tang, X. Han, L. Zhu, N. Wang, Degradation of bisphenol A by hydrogen peroxide activated with $CuFeO_2$ microparticles as a heterogeneous Fenton-like catalyst: Efficiency, stability and mechanism, Chemical Engineering Journal, 236(2014) 251-262.

[10] G. C. Allen, M. T. Curtis, A. J. Hooper, P. M. Tucker, X-Ray photoelectron spectroscopy of iron–oxygen systems, J. Chem. Soc. Dalton Trans. (1974) 1525.

[11] G. Ertl, K. Wandelt, Electron spectroscopic studies of clean and oxidized iron, Surf. Sci. (1975) 50, 479.